

Magnetic Behavior in RRh_3X ($R = \text{rare earths}$; $X=B, C$) Compounds

Devang A. Joshi* and Neeraj Kumar, A. Thamizhavel and S. K. Dhar
*Department of Condensed Matter Physics and Materials Science,
Tata Institute of Fundamental Research, Colaba, Mumbai 400 005, India.*

We report on the magnetic behavior of RRh_3B ($R = \text{La, Ce, Pr, Nd, Gd, Tb and Tm}$) and RRh_3C ($R = \text{La, Ce, Pr and Gd}$) compounds crystallizing in the cubic perovskite type structure with space group $Pm\bar{3}m$. The heat capacity data on Pauli-paramagnetic $LaRh_3B$ and $LaRh_3C$ indicate a high frequency vibrating motion of boron and carbon atoms in the unit cell. Ce is in α -like nonmagnetic state in both the compounds. Pr compounds show a dominant crystal field effect with a nonmagnetic singlet ground state in $PrRh_3B$ and a nonmagnetic quadrupolar doublet in $PrRh_3C$. Compounds with other rare earths order ferromagnetically at low temperatures except $TmRh_3B$ in which the zero field evolution of magnetic interactions is relatively more complicated. The electrical resistivity of $GdRh_3B$ decreases with increasing temperature in the paramagnetic state in the vicinity of T_C , which is rarely seen in ferromagnets. The behavior is discussed to be arising due to the short range spin fluctuation and a possible contribution from Fermi surface geometry.

PACS numbers: 75.50.Cc, 74.25.Ha and 71.70.Ch

Keywords: Crystal Field, RRh_3B , RRh_3C , Ferromagnetism and Spin fluctuation

I. INTRODUCTION

The existence of a large number of borides and carbides of rare earth compounds forming in the anti-perovskite structure is well known [1, 2]. Boron and carbon occupy the body-centered $(\frac{1}{2}, \frac{1}{2}, \frac{1}{2})$ position of the FCC unit cell in these compounds. Dhar et al. had reported the synthesis of RPd_3B_x ($0 \leq x < 1$) by alloying boron with RPd_3 ($R = \text{rare earth}$) compounds which have the $AuCu_3$ -type FCC structure [3]. The introduction of smaller atoms like boron and carbon leads in some cases to interesting changes in the physical properties of the parent compounds. For example, boron expands the unit cell and induces a change of valence from intermediate valent in $CePd_3$ to trivalent in $CePd_3B_x$ ($x > 0.25$) and from trivalent in $EuPd_3$ to mixed valent in $EuPd_3B_x$ ($x \sim 0.5$) [4, 5]. Evidence for charge ordering in $EuPd_3B$ was inferred from the variation of ^{151}Eu Mössbauer spectra with temperature [6]. The synthesis of perovskite type RRh_3B_x has also been reported in the literature [7, 8], though in this case only $CeRh_3$ is known to exist in $AuCu_3$ -type structure. The Curie-Weiss, paramagnetic behavior of the susceptibility of RRh_3B compounds between 300 and 77 K and ^{151}Eu Mössbauer measurements in $EuRh_3B$ indicating trivalent behavior of Eu ions have been reported [7]. Rogl and De-Long investigated some ternary borides for superconductivity but found $HfRh_3B_{1-x}$ and YRh_3B_{1-x} alloys non-superconducting down to 1.5 K [9]. A narrowing of the $5f$ band due to the hybridization between U $5f$ electrons and Rh d electrons was inferred in the perovskite URh_3B from heat capacity and susceptibility, further supported by band structure calculations [10]. More recently, cubic perovskite $MgNi_3C$ was found to become superconducting at $T \sim$

8 K [11]. In the recent past, RRh_3B_x compounds have been studied primarily with regard to the variation of hardness with boron content [12, 13]. In this communication, we report the magnetic properties of RRh_3B ($R = \text{La, Ce, Pr, Nd, Gd, Tb and Tm}$), based on the magnetization, heat capacity and electrical resistivity data measured down to 1.7 K. For comparison, RRh_3C compounds for $R = \text{La, Ce, Pr and Gd}$ were also synthesized and their magnetic behavior examined.

II. EXPERIMENTAL

The compounds were prepared by melting the stoichiometric amounts of constituent elements in an arc furnace on a water cooled cooper hearth under an inert atmosphere of argon. The purity of the starting material is R (99.9 wt. %), Rh (99.9 wt. %), B (99.5 wt. %) and C (99.9999 wt. %). The compounds were annealed at 800 °C for a week and checked with x-ray diffraction using $Cu K\alpha$ radiation. Magnetization measurements were carried out using a Quantum Design MPMS-5 superconducting quantum interference device magnetometer and Oxford Instruments vibrating sample magnetometer while the electrical resistivity was recorded on an automated home-built set up. The heat capacity was measured using a physical property measurement system (PPMS, Quantum Design).

III. RESULTS AND DISCUSSION

The RRh_3B and RRh_3C series of compounds form in a cubic perovskite structure with space group $Pm\bar{3}m$ [1]. The series of compounds form for almost all the rare earths in contrast to the parent RRh_3 , which forms only in case of Ce. Hence an additional atom (boron or carbon) is required to stabilize the perovskite structure.

*Electronic address: devang@tifr.res.in

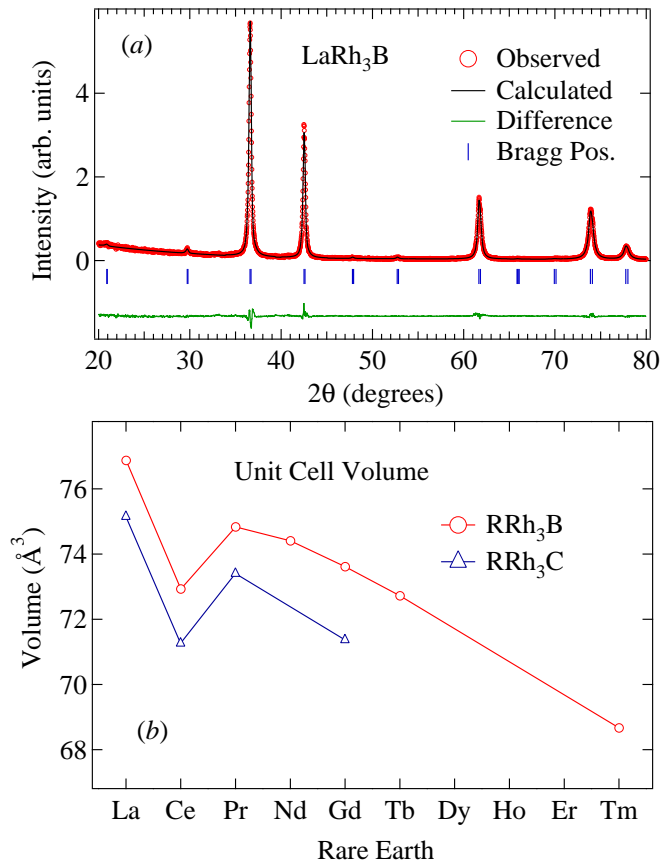


Figure 1: (Color online) (a) Powder x-ray diffraction pattern of LaRh_3B at room temperature. The solid line through the experimental data points is the Rietveld refinement profile calculated for the cubic LaRh_3B . The Bragg position and the difference of the observed and calculated profile is also shown. (b) Unit cell volume of RRh_3B and RRh_3C compounds plotted against their corresponding rare-earth constituents, the line joining the symbols is guide to the eye.

A minimum amount of boron is needed to stabilize the RRh_3B_x phase, the magnitude of x depends upon the rare earth R [12]. We believe a similar situation should also hold for alloying with carbon. In order to confirm the phase homogeneity of RRh_3B and RRh_3C compounds prepared in this work, with proper lattice and crystallographic parameters, a Rietveld analysis of the observed x-ray patterns of all the compounds was done using the Fullprof program. The refined plot of LaRh_3B is shown in Fig. 1a. The obtained lattice parameters are presented in Table 1 and the corresponding unit cell volumes are plotted in Fig. 1b. The unit cell volume decreases as we move to higher rare earths in accordance with the lanthanide contraction. For CeRh_3B and CeRh_3C , however, the value is below that expected on the basis of lanthanide contraction, indicating an α -like nonmagnetic state of Ce ions in these compounds. The unit cell volume of RRh_3B is larger than that of the corresponding RRh_3C

Compound	Lattice Parameters	a (\AA)	T_C (K)	μ_{eff} (μ_B)	θ_P (K)
LaRh_3B		4.252	P-P	-	-
CeRh_3B		4.178	P-P	-	-
PrRh_3B		4.214	P	3.58	-7
NdRh_3B		4.206	Below 2	3.62	3
GdRh_3B		4.191	12	7.88	12
TbRh_3B		4.174	6	9.5	5
TmRh_3B		4.095	4	7.57	-1
LaRh_3C		4.22	P-P	-	-
CeRh_3C		4.146	P-P	-	-
PrRh_3C		4.187	P	3.58	-11
GdRh_3C		4.148	3.5	7.9	3

Table I: Lattice parameters, magnetic ordering temperature, effective moment and paramagnetic Curie temperature for RRh_3B and RRh_3C compounds. P-P: Pauli-paramagnetic and P: Paramagnetic.

compounds, and it may be due to the larger metallic radius of the boron atom (0.88 \AA) compared to that of the carbon atom (0.77 \AA).

A. LaRh_3B and LaRh_3C

We first discuss the behavior of nonmagnetic, reference compounds LaRh_3B and LaRh_3C . The magnetic susceptibilities of LaRh_3B and LaRh_3C are shown in Fig. 2a. Both the compounds exhibit a Pauli-paramagnetic behavior. There is an increase in the susceptibilities at low temperatures, which may be due to the paramagnetic impurity within the samples, arising from the presence of paramagnetic ions in the starting materials. In order to estimate the temperature independent susceptibility (χ_0) the modified Curie-Weiss law ($\chi = \chi_0 + N\mu_{eff}^2/3k_B(T - \theta_P)$) was fitted to the data, the various parameters have their usual meaning. The obtained values of χ_0 are 2.0×10^{-4} and 0.4×10^{-4} emu/mole with effective moment of 0.17 and 0.22 μ_B respectively for LaRh_3B and LaRh_3C . Such a low value of effective moment indicates that the upturn at low temperature is due to the presence of paramagnetic impurity ions. The value of χ_0 for LaRh_3C is much less than that of LaRh_3B . Considering the fact that the Pauli-paramagnetism arises from the conduction electron polarization, it is possible that replacing boron by carbon shifts the Fermi level to a region of low density of states. This is supported by the low temperature heat capacity data plotted as C/T vs T^2 in Fig. 2b. The magnitude of the electronic contribution γ , obtained by fitting the expression $C/T = \gamma + \beta T^2$ to the data, is 15 and 6 mJ/mole K^2 for LaRh_3B and LaRh_3C respectively. Since γ is proportional to the density of states at the Fermi level, a reduction in the value of γ for LaRh_3C indicates a decrease in the density of states $N(E_F)$ at the Fermi level. The magnitude of

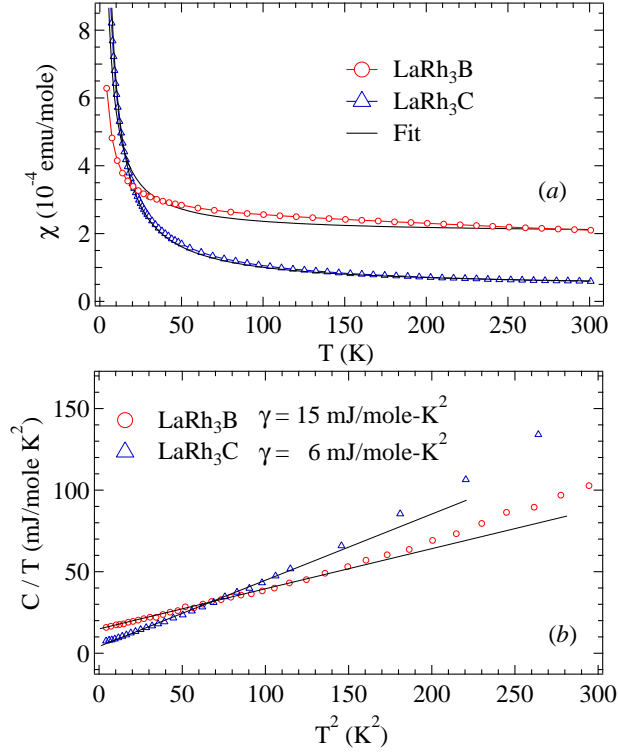


Figure 2: (Color online) (a) Magnetic susceptibility of LaRh_3B and LaRh_3C ; the solid lines represent a fit to the modified Curie-Weiss law. The line joining the data points is guide to eye. (b) C/T vs T^2 curve for LaRh_3B and LaRh_3C compounds. The solid lines represent a fit to an equation described in the text.

$N(E_F)$ can be obtained using the free electron relation

$$\gamma = \frac{2}{3} \pi^2 k_B^2 N(E_F) \quad (1)$$

where k_B is the Boltzmann constant. Substituting the value of γ for LaRh_3B and LaRh_3C , the density of states at the Fermi level is found to be $43.4 \text{ Ry}^{-1}\text{atom}^{-1}$ and $17.4 \text{ Ry}^{-1}\text{atom}^{-1}$ respectively.

The heat capacity of LaRh_3B and LaRh_3C between 1.7 and 150 K is plotted in Fig. 3a. The heat capacity of LaRh_3C is seen to be higher than that of LaRh_3B above 10 K but at lower temperatures the heat capacity of the latter dominates because of its higher electronic contribution. The thermal variation of the heat capacity of these two compounds could not be described by either the Debye or Einstein model separately, but could be well described by combined Einstein and Debye contributions as shown by the solid lines in Fig. 3a. The total heat capacity in such case is given by

$$C_{Tot} = \gamma T + (C_E + C_D) \quad (2)$$

where the first term represents the electronic contribution, The second term includes Einstein contribution C_E

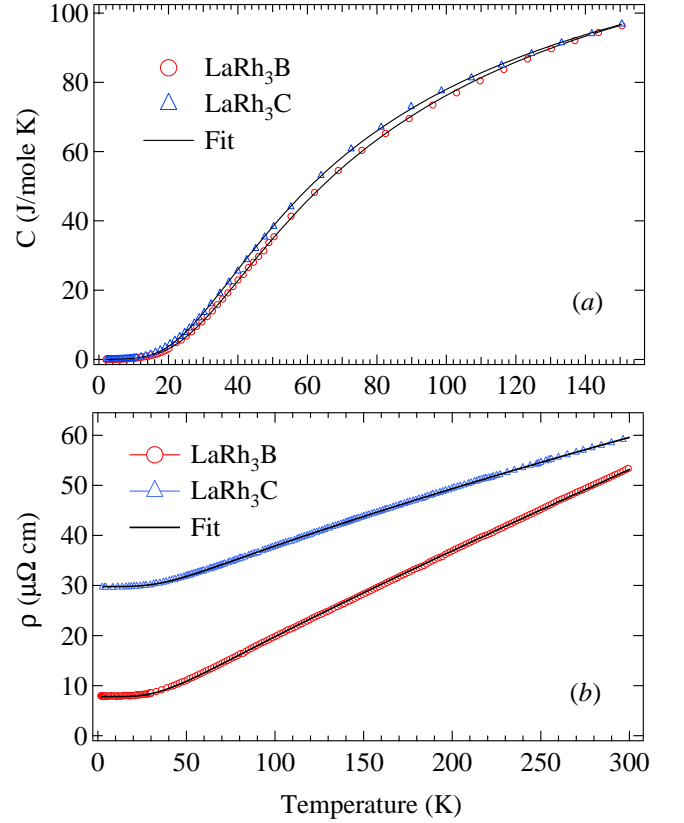


Figure 3: (Color online) (a) Heat capacity as a function of temperature for LaRh_3B and LaRh_3C with a fit to a combined Einstein and Debye contribution. (b) Resistivity behavior of LaRh_3B and LaRh_3C with a fit to Bloch-Grüneisen relation.

and Debye contribution C_D . The Einstein contribution is given by

$$C_E = \sum_{n'} 3n_{En'} R \frac{y^2 e^y}{(e^y - 1)^2} \quad (3)$$

where $y = \Theta_{En'}/T$, Θ_E is the Einstein temperature, n' is the summation over the different Einstein temperatures, R is the gas constant and n_E is the number of Einstein oscillators. The Debye contribution is given by

$$C_D = 9n_D R \left(\frac{T}{\Theta_D} \right)^3 \int_0^{\Theta_D/T} \frac{x^4 e^x dx}{(e^x - 1)^2} \quad (4)$$

where $x = \Theta_D/T$. Θ_D is the Debye temperature and n_D is the number of Debye oscillators. Iterative fit to the Eq. 2 was performed by using the values of electronic contribution γ as estimated above and fixing the number of atoms n_D and n_E for a particular fit, allowing both $\Theta_{En'}$ and Θ_D to vary as fitting parameters. A good fit to the heat capacity of LaRh_3B and LaRh_3C over the entire range of temperature was obtained by assigning three

Debye characteristic atoms ($n_D = 3$) with $\Theta_D = 287$ K plus two Einstein characteristic atoms ($n_{E1} = n_{E2} = 1$) with $\Theta_{E1} = 150$ K and $\Theta_{E2} = 569$ K for LaRh_3B and $\Theta_D = 272$ K, $\Theta_{E1} = 135$ K and $\Theta_{E2} = 569$ K for LaRh_3C . The total number of atoms ($n_D + n_E = 5$) accounts for the five atoms of each LaRh_3B and LaRh_3C compound. The description of heat capacity in terms of a combination of acoustic and optical contribution can readily be understood by assigning the Rh atoms in the unit cell to three Debye characteristic modes and the remaining to the Einstein modes. In the Einstein mode of vibration, $\Theta_{E1} \ll \Theta_{E2}$, since La is much larger in size (about 100 %) compared to B or C atoms, thus it can be expected to vibrate with a lower natural frequency compared to that of the latter ones. Hence Θ_{E1} corresponds to the vibration of La atoms and Θ_{E2} to that of B or C atoms. The change in the Debye temperature Θ_D and Einstein temperature Θ_{E1} from LaRh_3B to LaRh_3C can be understood to be due to the change in the lattice parameters, whereas a constant value of Θ_{E2} for both the compounds could not be understood but can tentatively be assigned to similar bonding strength of the boron and carbon with the neighboring atoms.

The resistivity of LaRh_3B exhibits a metallic like behavior down to 30 K (Fig. 3b), leveling off at low temperature with a residual resistivity of $7.8 \mu\Omega \text{ cm}$. The resistivity of LaRh_3C also shows a similar behavior but with a small negative curvature at low temperature (between 75 and 150 K) and a residual resistivity of $30 \mu\Omega \text{ cm}$. A possible source of negative curvature in the resistivity of nonmagnetic materials is due to the scattering of conduction electrons from s to d band [14]. The scattering is proportional to the density of states in the d band. Thus the substitution of C in place of B results in the shifting of the Fermi surface in the vicinity of d band. Also the resistivity of LaRh_3C is higher than that of LaRh_3B due to the decrease in the density of states at the Fermi level. The resistivity of both the compounds could be described by the modified Bloch-Grüneisen relation given by

$$\rho(T) = \rho_0 + 4\Theta_D R \left(\frac{T}{\Theta_D} \right)^5 \int_0^{\Theta_D/T} \frac{x^5 dx}{(e^x - 1)(1 - e^{-x})} - KT^3 \quad (5)$$

where $x = \Theta_D/T$, Θ_D is the Debye temperature, ρ_0 is the temperature independent residual resistivity and R and K are the coefficients of the phonon contribution to the resistivity (second term) and the Mott s - d interband scattering (third term) respectively. The fit to the resistivity curves yields $\Theta_D = 223$ K, $\rho_0 = 7.8 \mu\Omega \text{ cm}$, $R = 0.156 \mu\Omega \text{ cm K}^{-1}$ and $K = 0 \mu\Omega \text{ cm K}^{-3}$ for LaRh_3B and $\Theta_D = 226$ K, $\rho_0 = 30 \mu\Omega \text{ cm}$, $R = 0.11 \mu\Omega \text{ cm K}^{-1}$ and $K = 0.46 \cdot 10^{-7} \mu\Omega \text{ cm K}^{-3}$ for LaRh_3C . The finite value of the coefficient K for LaRh_3C supports the explanation of the small curvature in the resistivity curve proposed above. The Debye temperature in the Bloch-Grüneisen relation often differs from the value of Θ_D obtained from heat capacity data because the former takes

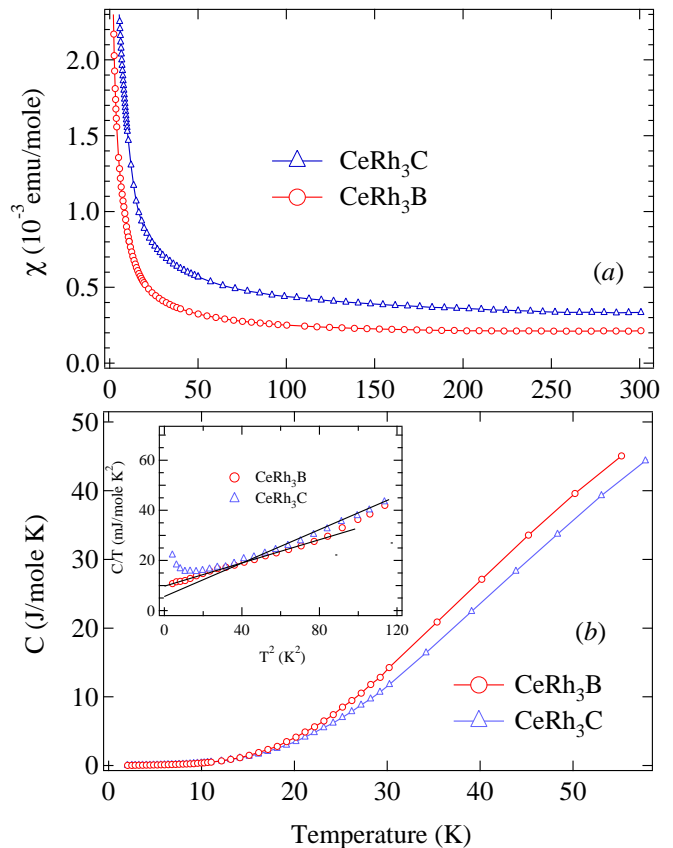


Figure 4: (Color online) (a) Magnetic susceptibility of CeRh_3B and CeRh_3C . The line joining the data points are guide to eye. (b) Heat capacity of CeRh_3B and CeRh_3C compounds with the inset showing C/T vs T^2 curve for both compounds. The solid lines in the inset represent a fit as described in text.

into account only the longitudinal phonons [15].

B. CeRh_3B and CeRh_3C

From a comparison of their lattice constants with neighboring La and Pr analogs, CeRh_3B and CeRh_3C are most likely intermediate valance compounds. This is well corroborated by their magnetic susceptibility, as shown in Fig. 4a. The susceptibility of CeRh_3B at 300 K is $\sim 2.3 \times 10^{-4}$ emu/mole and remains nearly temperature independent down to about 50 K, consistent with Pauli paramagnetic behavior. It is seen that the susceptibility of CeRh_3B is comparable to that of LaRh_3B and consistent with the non-magnetic nature of a nearly tetravalent or α -like state of Ce ions. The upturn in susceptibility at low temperatures is attributed to the presence of trace paramagnetic ions present in the starting constituents. A similar behavior is also observed in CeRh_3C with $\chi \sim 3.5 \times 10^{-4}$ emu/mole at 300 K, comparable to that of CeRh_3B . Even though the density of states at the Fermi

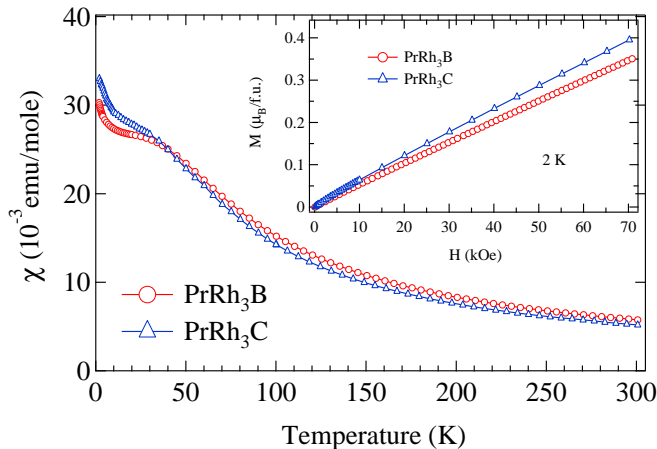


Figure 5: (Color online) Magnetic susceptibility of PrRh_3B and PrRh_3C , with the inset showing their magnetic isotherm at 2 K. The lines joining the data points are guide to eye.

level for CeRh_3B is higher than that of CeRh_3C (inferred from γ value as described below), the higher value of the susceptibility of CeRh_3C can be attributed to the slightly different $4f$ occupation in these two compounds.

The heat capacity of the compounds is shown in Fig. 4b. The heat capacity of CeRh_3B is less than that of CeRh_3C below ~ 11 K but exceeds the latter at higher temperatures. The behavior is in sharp contrast to that of the corresponding La compounds. The reason may be due to the changes in the Debye and Einstein characteristic temperatures of these two sets of compounds. The electronic contribution to the heat capacity estimated from the linear part of the C/T vs T^2 curve for CeRh_3B and CeRh_3C below 10 K is ~ 10 and 5 mJ/mole K^2 . The higher value for the boride is in agreement with the results on the corresponding La compounds.

C. PrRh_3B and PrRh_3C

The susceptibility of PrRh_3B and PrRh_3C is shown in Fig. 5. The susceptibility of both the compounds increases with decreasing temperature, followed by a nearly temperature-independent behavior at ≈ 25 K, followed by a further increase at lower temperatures. The magnetic isotherm of the compounds at 2 K (inset of Fig. 5a) shows a linear behavior up to 70 kOe, attaining a moment of ≈ 0.35 and $0.4 \mu_B/\text{f.u.}$ for PrRh_3B and PrRh_3C , respectively. The behavior of the susceptibility and a relatively low moment at 2 K in high fields indicates a paramagnetic state of these compounds with a strong crystal electric field effect. Such a behavior is not uncommon in the case of Pr compounds. The crystal field can split the $J = 4$ ground state of the Pr^{3+} ion, resulting in a nonmagnetic singlet[16] or a nonmagnetic quadrupolar doublet ground state (PrPb_3 , PrMg_3 and PrPtBi : [17, 18, 19]), if the exchange interactions do

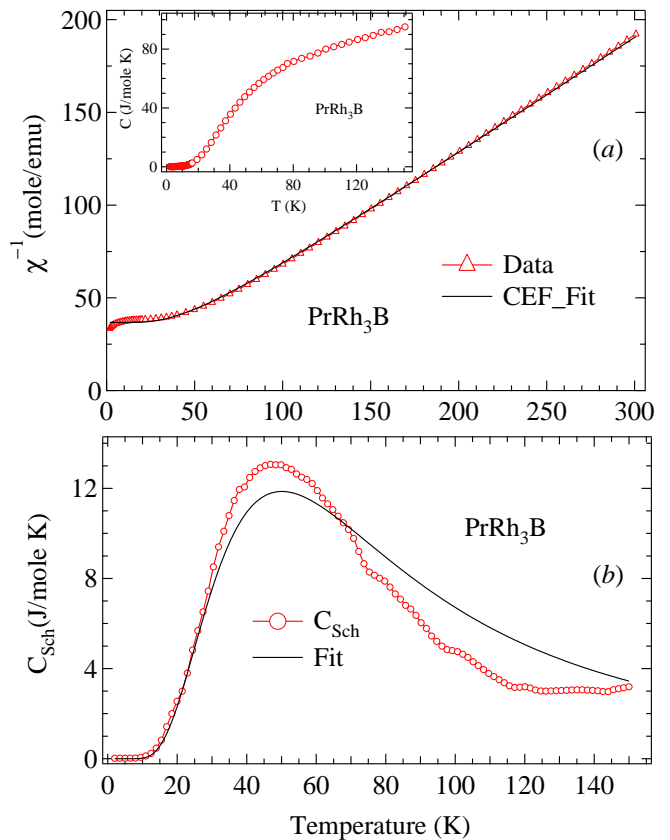


Figure 6: (Color online) (a): Inverse susceptibility as a function of temperature for PrRh_3B . The solid line through the data points represent a fit to CEF model as described in text. The inset shows the heat capacity of PrRh_3B . (b): Schottky contribution to the heat capacity of PrRh_3B with a solid line representing the theoretically simulated Schottky curve.

not exceed a certain critical value [20]. Such nonmagnetic ground states would give rise to a temperature-independent, Van-Vleck susceptibility at low temperatures. Hence the nearly temperature-independent behavior of the susceptibility (Fig. 5a) at $T \approx 25$ K for both the compounds arises from a nonmagnetic ground state. The upturn in the susceptibility at low temperatures is due to some trace paramagnetic impurities in the compounds. The fitting of the Curie-Weiss law to the inverse susceptibility furnishes an effective moment of $3.58 \mu_B$ for both compounds, equal to the theoretically expected value for the Pr^{3+} ion. The paramagnetic Curie temperatures are -7 and -11 K for PrRh_3B and PrRh_3C , respectively. The negative values are normally taken to imply an antiferromagnetic type of interaction, but since there is no magnetic transition down to 1.8 K they must result from crystal electric field effect. This is in contrast with the ferromagnetic interaction present in rest of the compounds with magnetic rare earth ions R.

The heat capacities of PrRh_3B and PrRh_3C are shown

as insets to Fig. 6a and Fig. 7a, respectively. The behavior is similar to that of a nonmagnetic compound. The Schottky contribution to the heat capacity of both the compounds was isolated by subtracting the heat capacity of the La analogue, after taking into account the slight difference in the atomic masses of La and Pr, and is shown in Fig. 6b and Fig. 7b, respectively. Both the compounds show a Schottky peak in their heat capacity arising from the thermal variation of the fractional occupation of the crystal electric field levels.

A set of CEF levels which reproduce the Schottky heat capacity reasonably well may plausibly be taken to represent the actual CEF splitting in these two compounds. Towards this goal the susceptibility of the two compounds was analyzed on the basis of a CEF model including the exchange parameter. Crystal field analysis was done taking into account the cubic symmetry of the Pr^{3+} ion in PrRh_3B and PrRh_3C . The CEF Hamiltonian for a cubic point group symmetry is given by [21]

$$H_{CEF}^{cub.} = B_4^0 (O_4^0 + 5O_4^4) + B_6^0 (O_6^0 - 21O_6^4) \quad (6)$$

where B_l^m and O_l^m are the CEF parameters and the Stevens operators, respectively. The diagonalization of the above Hamiltonian was done using the computer simulation to fit the inverse susceptibility of the compounds, as shown in Fig. 6a and 7a respectively. The CEF parameters obtained from the fit are $B_4^0 = -0.079$ K and $B_6^0 = 0.0005$ K for PrRh_3B and $B_4^0 = 0.0121$ K and $B_6^0 = -0.00135$ K for PrRh_3C . The susceptibility could be fitted to a set of values of the crystal electric field parameters, but only those parameters are taken into account which could also fit the experimentally obtained Schottky anomaly as well. The crystal field split energy levels obtained from CEF parameters are shown in Fig. 8. The ground state for PrRh_3B was found to be a singlet whereas that of PrRh_3C is a doublet. Since the carbide is not ordering magnetically at least down to 1.8 K, the ground state is most likely a quadrupolar nonmagnetic doublet. These energy levels were used to calculate the Schottky contribution from the equation

$$C_{Sch}(T) = R \left[\frac{\sum_i g_i E_i^2 e^{-E_i/T} \sum_i g_i E_i^2 e^{-E_i/T} - [\sum_i g_i E_i e^{-E_i/T}]^2}{T^2 [\sum_i g_i e^{-E_i/T}]^2} \right] \quad (7)$$

where R is the gas constant, E_i is the CEF energy level in units of temperature and g_i the corresponding degeneracy. The curves obtained are shown in Fig. 6b and Fig. 7b, respectively for PrRh_3B and PrRh_3C . There is only a qualitative agreement between the observed and the calculated Schottky contribution. The discrepancy may arise due to the uncertainty in isolating the pure phonon contribution as the phonon spectra of PrRh_3B and PrRh_3C may not be identical to that of LaRh_3B and LaRh_3C , respectively. The peak positions, however, nearly match indicating that our inferred CEF level scheme is fairly close to the actual splitting in both compounds scheme.

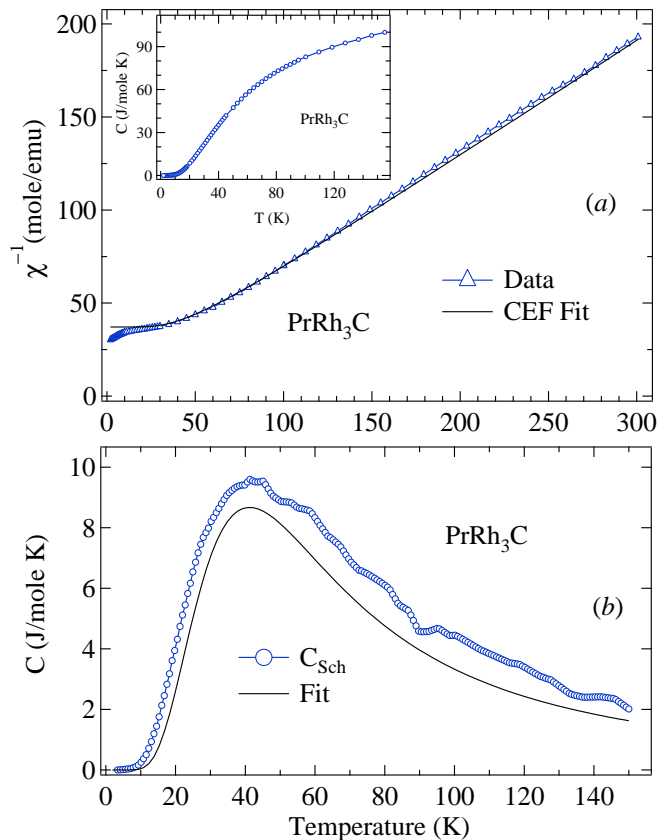


Figure 7: (Color online) (a): Inverse susceptibility as a function of temperature for PrRh_3C . The solid line represent a fit to CEF model as described in text. The inset shows the heat capacity behavior of PrRh_3C . (b): Schottky contribution to the heat capacity of PrRh_3C with solid line representing the simulated Schottky curve.

D. GdRh_3B and GdRh_3C

The results on GdRh_3B and GdRh_3C are presented as Gd is an S -state ion and the CEF effects are negligible in the first order approximation. The magnetic susceptibility of both the compounds under zero field cooled (ZFC) and field cooled (FC) conditions at 100 Oe is shown in Fig. 9a. GdRh_3B and GdRh_3C order ferromagnetically at 12 and 3.5 K respectively. Substituting carbon in place of boron decreases the ordering temperature substantially. Since the Gd^{3+} ion is unaffected by the crystal field, the lower magnetic ordering temperature in the carbide is likely due to a decrease in the density of states at the Fermi level, inferred from the magnitude of γ in La and Ce compounds when boron is replaced by carbon. In case of GdRh_3B , the susceptibilities under FC and ZFC conditions coincide with each other, whereas a slight difference is observed for GdRh_3C . The behavior of the magnetic isotherm of both the compounds at 2 K (Fig. 9b) is as expected

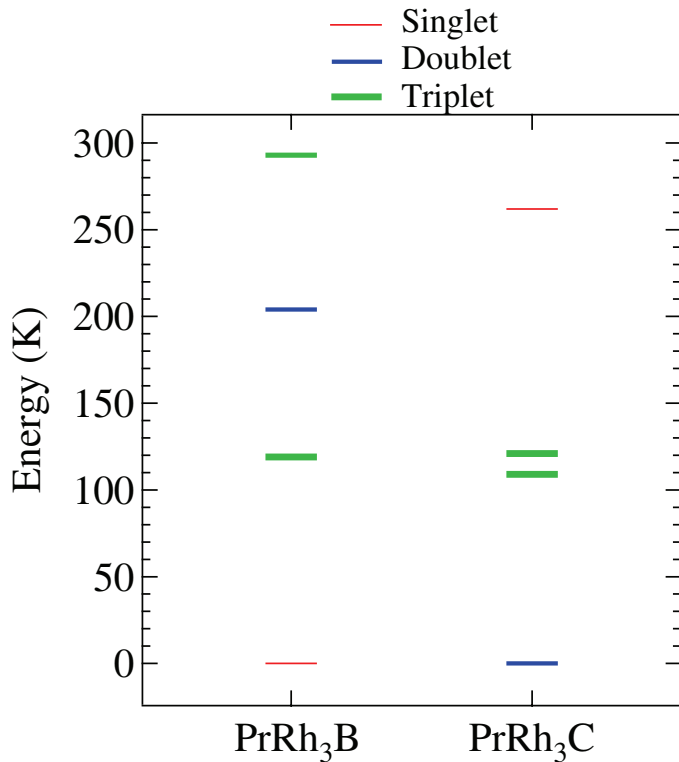


Figure 8: (Color online) Crystal field split energy levels of PrRh_3B and PrRh_3C estimated from a CEF fit to inverse susceptibility.

for a ferromagnetically ordered compound. The magnetization for GdRh_3B increases sharply at low fields and saturates quickly, compared to that of GdRh_3C which saturates above 40 kOe. The saturation moments obtained for GdRh_3B and GdRh_3C respectively are 6.87 and 6.84 $\mu_B/\text{f.u.}$ at 2 K and 80 kOe, close to the theoretically expected value of the Gd^{3+} ion ($7 \mu_B$).

The heat capacity of both the compounds shows an anomaly at the magnetic ordering temperature. (Fig. 10a). In GdRh_3C the heat capacity shows a broad shoulder between 2 and 5 K followed by a sharp peak at 2.2 K in contrast to a relatively sharp upturn in GdRh_3B . The heat capacity data in GdRh_3C suggest a relatively complicated evolution of the magnetic interactions leading to full magnetic ordering at 2.2 K, which may be responsible for the slight difference in the ZFC and FC plots and for the relatively slow saturation of the magnetization in GdRh_3C at 2 K. As regards the latter point it may also be noted that the isothermal magnetization plot at 2 K is taken close to the magnetic ordering temperature. The magnetic contribution to the heat capacity of GdRh_3B was isolated using the procedure described above and the entropy at 30 K is 17.6 J/mole K, close to the expected value of $R \ln(2J + 1)$.

The resistivity of both the compounds is shown in Fig. 10b. with the inset showing the low temperature part.

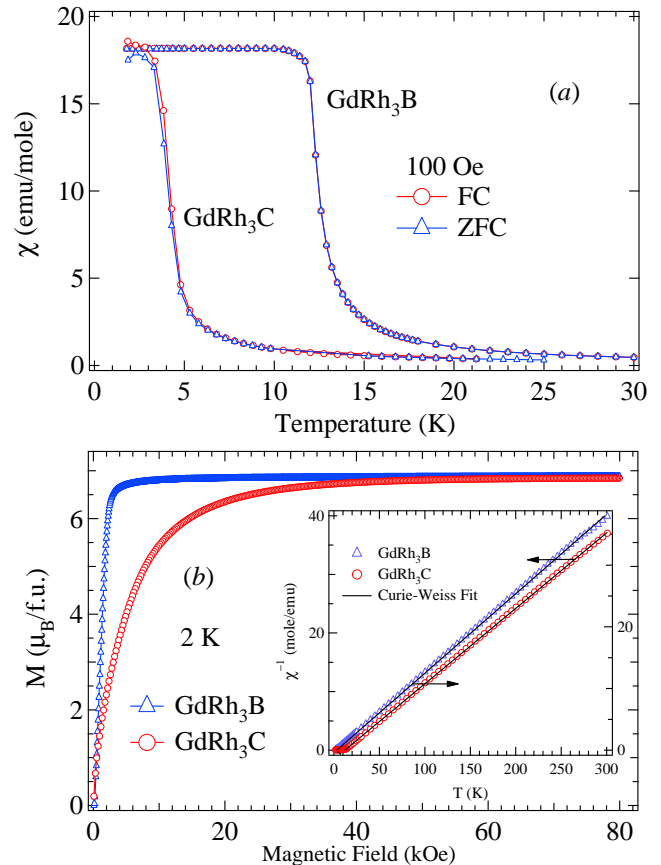


Figure 9: (Color online) a: Magnetic susceptibility of GdRh_3B and GdRh_3C under zero field cooled and field cooled conditions. b: Magnetic isotherm of both the compounds at 2 K. The inset shows the inverse magnetic susceptibility of both the compounds with solid lines representing a Curie-Weiss fit.

The resistivity at high temperature shows a metallic behavior for both the compounds. For GdRh_3B the resistivity decreases from $\approx 90 \mu\Omega \text{ cm}$ at room temperature to $\approx 10 \mu\Omega \text{ cm}$ at 2 K in contrast to a significant drop in the resistivity of GdRh_3C from $\approx 180 \mu\Omega \text{ cm}$ at room temperature to $\approx 24 \mu\Omega \text{ cm}$ at 2 K. The higher resistivity of GdRh_3C compared to that of GdRh_3B supports the low density of states at the Fermi level in the former. At low temperature (inset of Fig. 10b) the resistivity of GdRh_3C shows a drop at the ordering temperature of the compound due to the gradual disappearance of the spin disorder resistivity. Interestingly the resistivity of GdRh_3B increases below 20 K up to the ordering temperature in the paramagnetic regime showing a cusp at the ordering temperature. Such a behavior of resistivity is common in antiferromagnets but very rarely seen in ferromagnets (eg., *c* direction of Gd metal, $\text{La}(\text{Fe}, \text{Si})_{13}$ and Fe_3Pt [22, 23, 24]). In the case of antiferromagnets it has been argued that as one approaches T_C from above, the growth of spin correlations lead to large-wave-vector q fluctuations (q : magnetic reciprocal

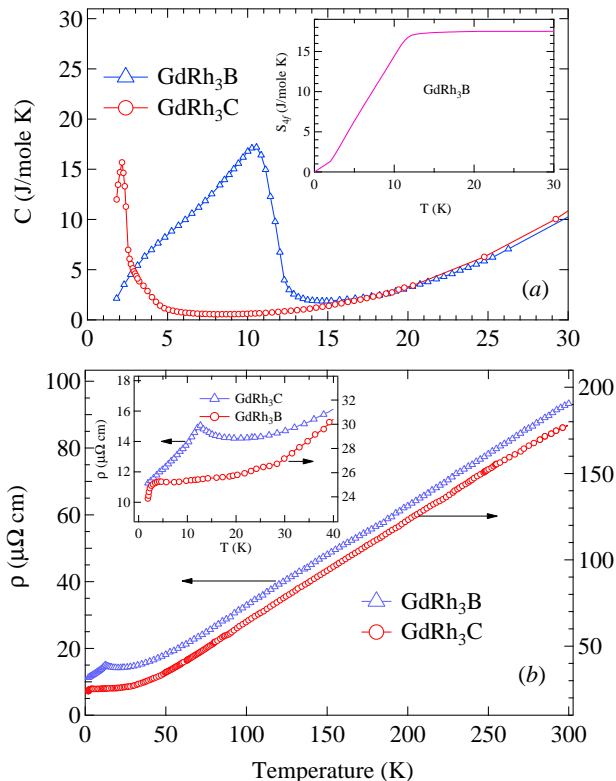


Figure 10: (Color online) a: Low temperature heat capacity of GdRh_3B and GdRh_3C with the inset showing the calculated entropy for GdRh_3B . The line joining the data points are guide to eye. b: Resistivity behavior of GdRh_3B and GdRh_3C . The inset shows the low temperature part for both compounds. The arrows in both plots point to their respective scales.

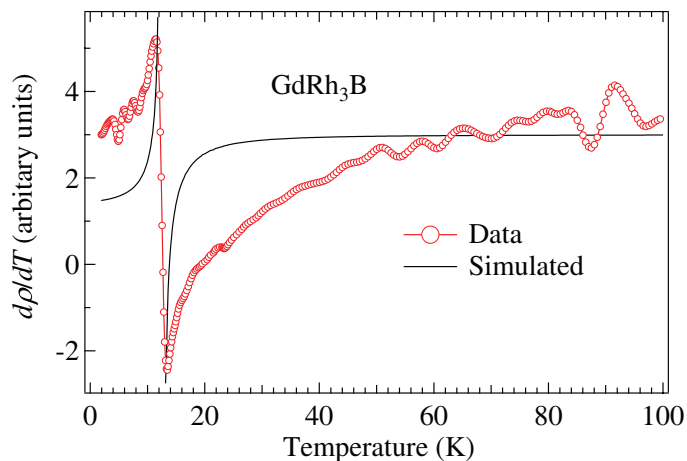


Figure 11: (Color online) The first derivative of resistivity for GdRh_3B indicating a discontinuity at the ordering temperature and the solid line represents the theoretically simulated curve to support the behavior.

lattice vector) which increase the resistivity due to spin fluctuations as the temperature is decreased [25]. In ferromagnets, such behavior arises for various reasons, in case of $\text{La}(\text{FeSi})_{13}$ and Fe_3Pt the behavior arises due to the lattice softening associated with the Invar effect [26]. In case of Gd metal, the presence of small Fermi surface caliper in the c direction is responsible for the experimentally observed cusp in the resistivity along the c -axis [27, 28]. In addition to these effects, a theory by Kim [30] shows that an anomaly in the resistivity of the ferromagnetic metals or alloys at their ordering temperature arises due to the scattering of conduction electrons by short range spin fluctuations. Kawatra *et. al.* [29] using Kims theory [30] showed that presence of short range spin fluctuations cause a sharp discontinuity in the $d\rho/dT$ curve at the ordering temperature of the compound. The $d\rho/dT$ curve for GdRh_3B is shown in Fig. 11. It shows a sharp anomaly and a change in sign at the ordering temperature. Also the sharp anomaly in $d\rho/dT$ curve is well described by the the simulated curve (Fig. 11) using equations described by Kim [30]. This shows that short range spin fluctuations is the major cause for the cusp at the ordering temperature. Here we do not rule out the contribution from Fermi surface geometry, but a proper estimation of the Fermi surface and single crystal data are required to confirm.

E. NdRh_3B , TbRh_3B and TmRh_3B

The magnetic behavior of NdRh_3B , TbRh_3B and TmRh_3B is described next. The selection of a Tm compound from the series is because of its expected behavior to form nonmagnetic singlet ground state. In the paramagnetic state the fit of the Curie-Weiss law (not shown) to the susceptibility of NdRh_3B and TbRh_3B furnishes $\mu_{eff} = 3.62$ and $9.5 \mu_B$ and paramagnetic Curie temperature $\theta_P = 3$ and 5 K, respectively. The effective moments are close to their respective free ion moment, and the positive value of θ_P indicates the ferromagnetic type of interaction between the moments. The ferromagnetic nature of the magnetic ordering in TbRh_3B below 6 K and below 2 K in NdRh_3B is apparent from the low-field magnetization plots shown in Fig. 12a. A slight deviation between the ZFC and FC plots below 4 K in TbRh_3B and the field dependence of the isothermal magnetization at 2 K (Fig. 12b) suggests the presence of magnetic anisotropy arising from the CEF effects. On the other hand both the FC and ZFC curves of NdRh_3B in the paramagnetic state coincide with each other as expected. The magnetic isotherm for TbRh_3B (Fig. 12b) is typical of a ferromagnetically ordered compound, with a moment of $7.8 \mu_B/\text{f.u.}$ at 2 K and 120 kOe, close to the saturation moment of $9 \mu_B/\text{Tb}$. Similar behavior is seen in NdRh_3B at 2 K, with a magnetic moment of $\approx 2.3 \mu_B/\text{f.u.}$ at 120 kOe. The electrical resistivity of TbRh_3B (Fig. 14) shows a clear anomaly at 6 K, decreasing sharply at lower temperatures. However, the heat capacity shows a sharp

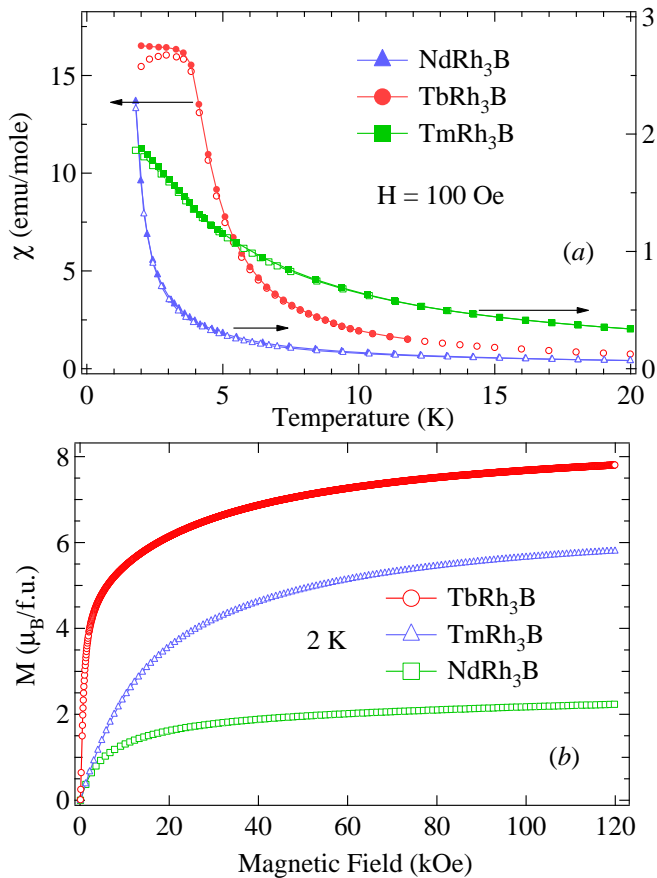


Figure 12: (Color online) a: Magnetic susceptibility of NdRh_3B , TbRh_3B and TmRh_3B under ZFC (unfilled symbols) and FC (Filled symbols) conditions. The arrows indicates their respective axis. b: Magnetic isotherms of the same compounds at 2 K.

peak at 3.6 K (Fig. 13b). In the paramagnetic state the heat capacity in zero field exhibits a relatively long tail suggestive of extended short range order in the paramagnetic state. Therefore, the anomaly at 6 K in the resistivity of TbRh_3B may signify the onset of strong short range order than truly long range magnetic ordering. The ferromagnetic nature of the magnetic correlations is further suggested by the effect of magnetic field (40 kOe) on the heat capacity of TbRh_3B (Fig. 13b). The peak at 3.6 K vanishes and the entropy due to the ordering is shifted to higher temperatures. The heat capacity of NdRh_3B (Fig. 13a) shows an upturn below 5 K attaining a value of nearly 3 J/mole K at the lowest temperature of 1.7 K. The upturn is a precursor to the magnetic ordering at lower temperature. The resistivity of NdRh_3B shows a metallic behavior down to 2 K (Fig. 14) with no signature of low temperature magnetic ordering.

The susceptibilities of TmRh_3B under ZFC and FC modes (Fig. 12a) nearly coincide with each other. Unlike the Gd, Tb and Nd analogs there is no sharp rise but a change in the slope at ≈ 4 K. The magnetic isotherm

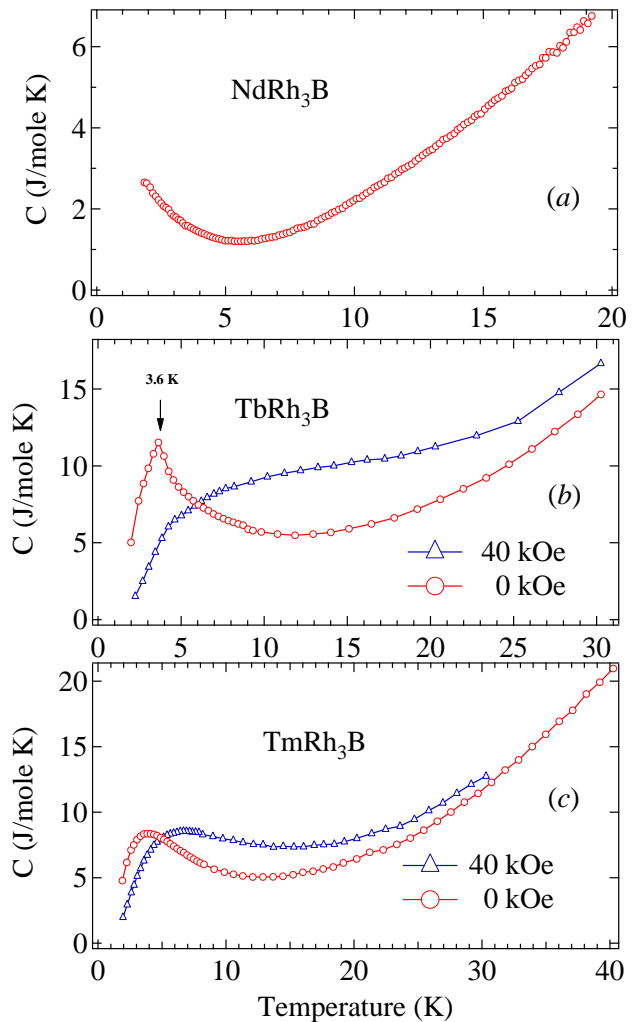


Figure 13: (Color online) Heat capacity data of NdRh_3B , TbRh_3B and TmRh_3B . Heat capacity of TbRh_3B and TmRh_3B in a field of 40 kOe are also shown. The line joining the data points are guide to eye.

of the compound at 2 K (Fig. 12a) has a behavior typical of ferromagnets, with a magnetic moment of $\approx 5.8 \mu_B/\text{f.u.}$ at 120 kOe. The Curie-Weiss fit to the inverse susceptibility in the paramagnetic region yields $\mu_{eff} = 7.6 \mu_B$ and $\theta_P = -1$ K. The heat capacity and resistivity data are shown in Fig. 13c and 14. The heat capacity shows a broad peak centered at ≈ 4 K with a long tail in the paramagnetic region similar to that of TbRh_3B . The effect of the applied magnetic field on the heat capacity of TmRh_3B is similar to that in TbRh_3B , the broad peak getting shifted to higher temperature by a few degrees. The resistivity too shows a drop at ≈ 4 K but the drop in the resistivity is not so significant, it just drops by just $0.08 \mu\Omega \text{ cm}$ between 4 and 2 K. The low-field susceptibility together with magnetic heat capacity and resistivity measurements indicate the presence of a

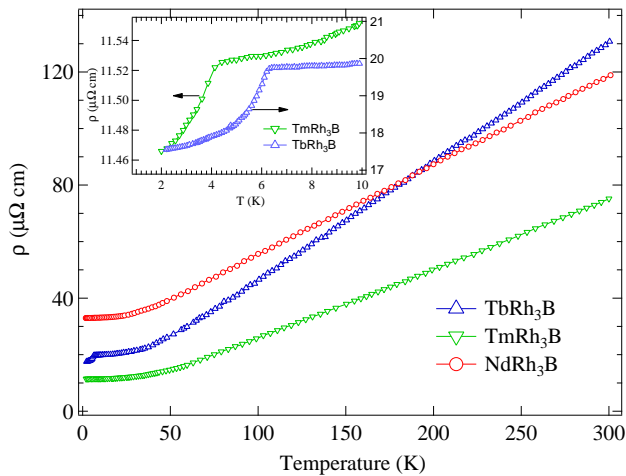


Figure 14: (Color online) Resistivity behavior of NdRh_3B , TbRh_3B and TmRh_3B . The inset shows the low temperature part for TbRh_3B and TmRh_3B . The lines connecting the data points is guide to the eye.

complicated magnetic structure.

IV. CONCLUSION

In conclusion, we have studied the magnetic behavior of RRh_3B ($\text{R} = \text{La}, \text{Ce}, \text{Pr}, \text{Nd}, \text{Gd}, \text{Tb}$ and Tm) and RRh_3C ($\text{R} = \text{La}, \text{Ce}, \text{Pr}$ and Gd) compounds. The compounds form in perovskite type cubic structure with space group $\text{Pm}\bar{3}\text{m}$. LaRh_3B and LaRh_3C show Pauli-paramagnetic behavior. Substitution of C in place of B causes decrease in the density of states at the Fermi level. Ce is in α -like state in both the compounds. Pr compounds shows a dominant crystal field effect with a non-magnetic singlet ground state in PrRh_3B and a nonmagnetic quadrupolar doublet in PrRh_3C . Compounds with other rare earths order ferromagnetically at low temperatures. Resistivity of GdRh_3B shows the presence of short range spin fluctuations, which is rarely seen in ferromagnets. TbRh_3B and TmRh_3B order ferromagnetically at 6 and 4 K respectively. NdRh_3B has an ordering temperature below 2 K.

- [1] H. Holleck, *J. Less-Comm. Met.*, **52**, 167 (1977).
- [2] P. Rogl and H. Nowotony, *J. Less-Comm. Met.*, **67**, (1979) 41.
- [3] S.K. Dhar, S.K. Malik and R. Vijayaraghavan, *Mater. Res. Bull.* **16**, 1557(1981).
- [4] S.K. Dhar, S.K. Malik and R. Vijayaraghavan, *Phys. Rev. B* **24**, 6182, (1981).
- [5] S.K. Dhar, S.K. Malik, D. Rambabu and R. Vijayaraghavan, *J. Appl. Phys.* **53**, (1982) 8077.
- [6] S.K. Dhar, R. Nagarajan, S.K. Malik, R. Vijayaraghavan, M.M. Abd-Elmeguid and H. Micklitz, *Phys. Rev. B* **29**, 5953 (1984).
- [7] S.K. Dhar, Ph.D thesis, Univ. of Mumbai, 1982.
- [8] H. Takei and T. Shishido, *J. Less-Comm. Met.* **97**, 223 (1984).
- [9] P. Rogl and L. DeLong, *J. Less-Comm. Met.* **91**, 97 (1983).
- [10] B.D. Dunlap, G.W. Crabtree, J.D. Jorgensen, H.A. Kierstead, D.D. Koelling, W.K. Kwok, D.J. Lam, S.K. Malik, A.W. Mitchell and S.C. Strite, *Phys. Rev B* **39**, 5640 (1989).
- [11] T. He, Q. Huang, A.P. Ramirez, Y. Wang, K.A. Regan, N. Rogado, M.A. Hayward, M.K. Haas, J.S. Slusky, K. Inumara, H.W. Zandbergen, N.P. Ong, R.J. Cava, *Nature*, **411**, 54 (2001).
- [12] T. Shishido, Jinhua Ye, K. Kudou, S. Okada, K. Obara, T. Sugawara, M. Oku, K. Wagatsuma, H. Horiuchi, T. Fukuda, *J. Alloys Compd.* **291**, 52 (1999).
- [13] T. Shishido, T. Sasaki, K. Kudou, S. Okada, A. Yoshikawa, J.M. Ko, J. Ye, I. Higashi, M. Oku, H. Horiuchi, T. Fukuda, S. Kohiki, K. Nakajima, *J. Alloys Compd.* **335**, 191 (2002).
- [14] N. F. Mott and F. Jones, *The Theory of the Properties of Metals and Alloys*, Oxford University Press London.
- [15] E. S. R. Gopal, *Specific Heat at Low Temperatures*, (Plenum Press), **Chap. 2** (1966) and references therein.
- [16] K.H.J. Buschow, de Wijn, H. W. and van Diepen, A. M., *J. Chem. Phys.* **50** 137(1969).
- [17] E. Bucher, K. Andres, A.C. Grossard and J.P. Maita, *J. Low Temp. Phys.* **2**, 322 (1972).
- [18] H. Tanida, H. S. Suzuki, S. Takagi, H. Onodera and K. Tanigaki, *J. Phys. Soc. Jpn.* **75** (2006) 073705.
- [19] H. Suzuki, M. Kasaya, T. Miyazaki, Y. Nemoto and T. Goto, *J. Phys. Soc. Jpn.* **66** (1997) 2566.
- [20] B. Bleaney: *Proc. Roy. Soc. A* **276** (1963) 19.
- [21] M. T. Hutchings, in *Solid State Physics*, F. Seitz and D. Turnbull, Eds. (Academic Press Inc., New York, 1964), Vol. 16, p.227.
- [22] K. Maezawa, K. Mori, K. Sato, Y. Saito and S. Wakabayashi, *J. Phys. Soc. Jpn.* **43** (1977) 1815.
- [23] T.T.M. Palstra, J.A. Mydosh, G.J. Nieuwenhuys, A.M. van der Kraan, *J. Magn. Magn. Mater.* **36** (1983) 290.
- [24] M. Viard and G. Gavoille, *J. Appl. Phys.* **50** (1979) 1828.
- [25] I. Balberg, *Physica* **91B**, **71** (1977).
- [26] R. J. Weiss, *Proc. Phys. Soc.* **82** (1963) 281.
- [27] D. J. W Geldart, T. G. Richard, *Phys. Rev. B* **12**, 5175 (1975).
- [28] A. J. Freeman, in *Magnetic Properties of Rare Earth Metals*, edited by R. J. Elliot (Plenum, London, 1972).
- [29] M. P. Kawatra, S. Skalski, J. A. Mydosh and J. L. Budnick, *Phys. Rev. Lett.* **23**, 83 (1969).
- [30] D. J. Kim, *Progr. Theoret. Phys.* **31**, 921 (1964)